Electronic Supplementary Information to

Properties of gaseous *closo*-$[B_6X_6]^{2-}$ dianions (X = Cl, Br, I)

Markus Rohdenburg,[a] Zheng Yang,[b] Pei Su,[c] Eduard Bernhardt,[d] Qinqin Yuan,[b] Edoardo Apra,[e] Simon Grabowsky,[f] Julia Laskin,[c] Carsten Jenne,[d] Xue-Bin Wang,*[b] and Jonas Warneke*[g,h]

a Institut für Angewandte und Physikalische Chemie, Fachbereich 2-Biologie/Chemie, Universität Bremen, 28359 Bremen, Germany.

b Physical Sciences Division, Pacific Northwest National Laboratory, Richland, WA 99352, USA.

c Department of Chemistry, Purdue University, West Lafayette, IN 47907, USA.

d Anorganische Chemie, Fakultät für Mathematik und Naturwissenschaften, Bergische Universität Wuppertal, 42119 Wuppertal, Germany.

e Environmental Molecular Sciences Laboratory, Pacific Northwest National Laboratory, Richland, WA 99352, USA.

f Departement für Chemie und Biochemie, Universität Bern, 3012 Bern, Switzerland.

g Wilhelm-Ostwald-Institut für Physikalische und Theoretische Chemie, Universität Leipzig, 04103 Leipzig, Germany.

h Leibniz Institute of Surface Engineering (IOM), Department Functional Surfaces, 04318 Leipzig, Germany

Table S1. ADE and VDE values for $[B_6X_6]^{2-}$ (X=Cl,Br) derived from various theoretical models and optimized geometries. In case of different methods used for geometry optimization and energy evaluation, both methods are stated as Energy//Geometry. All calculations employed the aug-cc-pVTZ basis set. All energies are given in eV.

Energy // Geometry	CAM-B3LYP	CCSD// PBE0	CCSD(T)// PBE0	CCSD	CCSD(T)// CCSD	CCSD(T)// CAM-B3LYP	MP2	SCS-MP2// MP2	CCSD// MP2	CCSD(T)// MP2
$[B_6Cl_6]^{2-}$										
ADE	0.004	-0.034	-0.065	0.131	-	-	0.110	0.077	0.045	0.012
VDE	0.506	0.425	0.403	0.447	0.425	0.474	0.398	0.523	0.364	0.345
$[B_6Br_6]^{2-}$										
ADE	0.537	-	-	-	-	-	0.529	0.508	-	-
VDE	0.919	-	-	-	-	-	0.906	0.845	-	-

Table S2. Selected B-X bond properties based on all-electron B3LYP-GD3BJ/6-311G** wave functions.

X =		Cl		Br		I	
Property		B6	B12	B6	B12	B6	B12
d / Å		1.838	1.807	1.989	1.969	2.189	2.192
δ		0.67	0.68	0.73	0.76	0.90	0.95
Q_{AIM} / e	B	+0.41	+0.51	+0.34	+0.39	+0.13	+0.11
	X	-0.74	-0.67	-0.67	-0.56	-0.46	-0.28
Q_{NPA} / e	B	-0.05	+0.01	-0.11	-0.08	-0.23	-0.23
	X	-0.29	-0.18	-0.23	-0.09	-0.10	+0.07

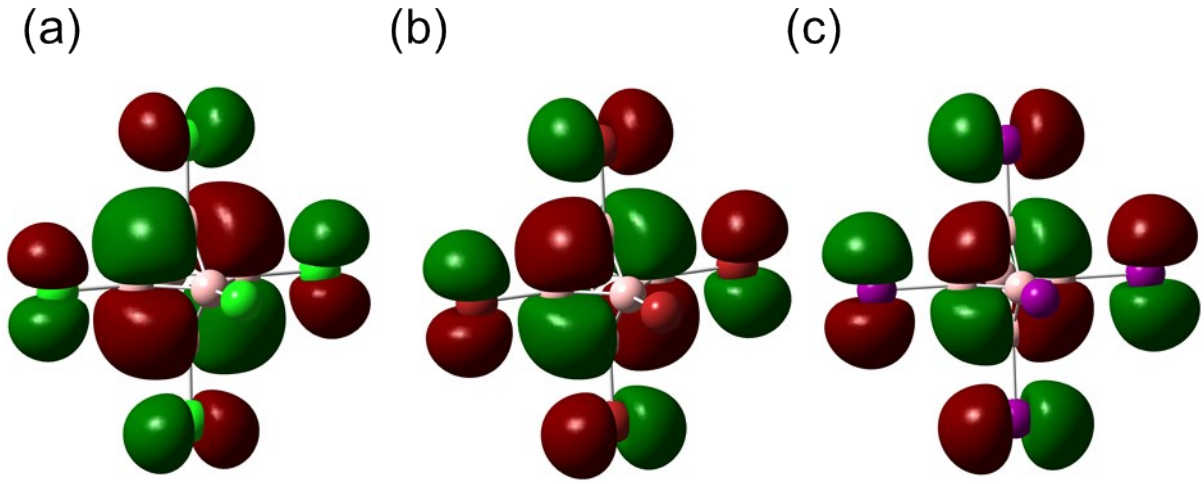

Figure S1. HOMO isosurface representations for the *closo*-hexaborate dianions (a) $[B_6Cl_6]^{2-}$, (b) $[B_6Br_6]^{2-}$ and (c) $[B_6I_6]^{2-}$ at an isovalue of 0.02 a.u. and calculated on HF/aug-cc-pVTZ//B3LYP-GD3BJ/aug-cc-pVTZ (SDD for I) level of theory. All HOMOs are triply degenerate. The HOMOs are of the same type as reported for $[B_6F_6]^{2-}$ (see ref. 65 in the main article) with both boron- and halogen-centered AOs participating in the HOMO.

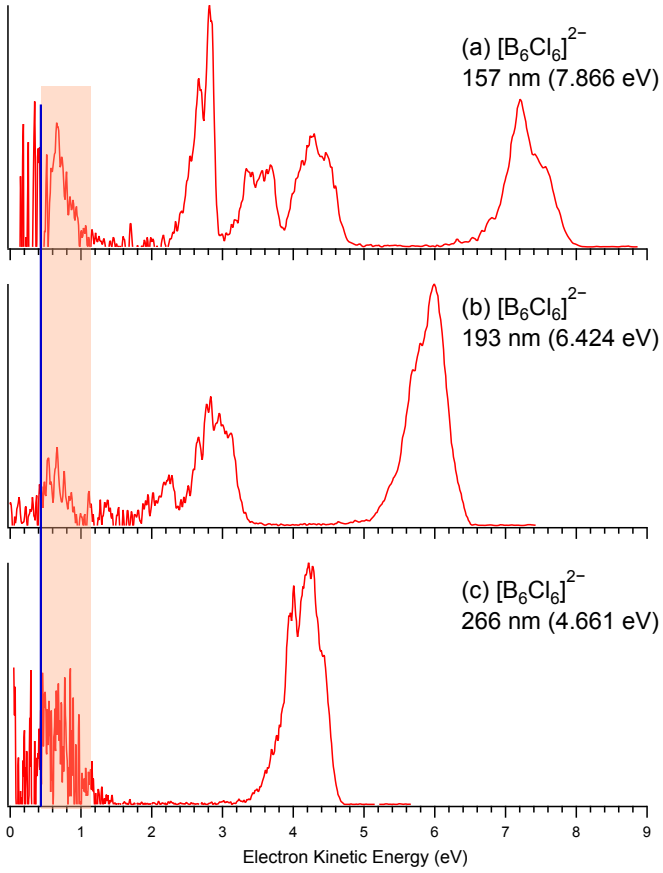

Figure S2. Kinetic energy PE spectra of $[B_6Cl_6]^{2-}$ obtained at 157, 193, and 266 nm. The vertical blue line depicts the RCB for the delayed detachment channel from the hot ion. The shaded region highlights the thermal bands at 157, 193, and 266 nm with the same kinetic energy.

To understand the presence of the band T, we need to note that electron binding energies (x-axes of spectra in Figure 2) are calculated by subtracting the kinetic energy of the detected electron from the laser energy (LE) applied for photodetachment. Therefore, if very low kinetic energy photoelectrons are detected, the corresponding signal appears at high binding energies in the spectra. However, this direct assignment of a kinetic electron energy to an actual binding energy is only adequate, if the detected electrons are the result of a direct photodetachment process (which is usually the case). However, a so called "thermal emission" can occur if a photon is absorbed by the anion and the energy is dissipated into vibrational modes instead of direct detachment of an electron. If the ion has a very low electron binding energy, like in the case of X=Cl, the "hot" ions may emit thermal electrons which appear as a band at high electron binding energies in the spectra. To clarify the case of band T in Figure 2, we examined the wavelength dependency of *closo*-$[B_6Cl_6]^{2-}$ PES spectra, see Figure S3. While band positions associated with directly photodetached electrons are independent of the laser wavelength, the band T changes and appears always at binding energies near the energy of the applied laser (same kinetic energy at different laser wavelength, see Figure S2 above). This confirms that responsible electrons are thermal electrons which do not origin from a direct photodetachment process but are emitted by the ion after photon

absorption. The band T can therefore be attributed to the special electronic property of the *closo*-$[B_6Cl_6]^{2-}$ on the borderline of MCA stability. In agreement with this, spectra of *closo*-$[B_6Br_6]^{2-}$ and *closo*-$[B_6I_6]^{2-}$ did not show such a spectral band.

Table S3: 0 K Enthalpies (in kJ/mol) for the three competing reactions shown in Figure 3 for all investigated *closo*-$[B_{12}X_{12}]^{2-}$ and *closo*-$[B_6X_6]^{2-}$. Two asterisks mark the experimentally observed dominant pathways and one asterisk an observed side reaction. Enthalpies for e^-, X^- and $X^\bullet$ loss were calculated using the model chemistry stated above the respective part of the table. For e^- loss, experimental values derived from PE spectroscopy (Table 1) are given in parentheses.

(a) B3LYP-GD3BJ/def2-TZVPP

Substituent X	$[B_{12}X_{12}]^{2-}$			$[B_6X_6]^{2-}$		
	e^- loss	$X^\bullet$ loss	X^- loss	e^- loss	$X^\bullet$ loss	X^- loss
F	129.1 (135)**	608	333	-181.5 (n.a.)	625	134
Cl	222.4 (245)	477	233**	-29.0 (-4.8)**	510	90
Br	251.3 (261)	422*	208**	21.0 (48)**	463	87*
I	207.9 (224)	362**	173*	66.7 (86)	411	85**

(b) B3LYP-GD3BJ/aug-cc-pVTZ

Substituent X	$[B_{12}X_{12}]^{2-}$			$[B_6X_6]^{2-}$		
	e^- loss	$X^\bullet$ loss	X^- loss	e^- loss	$X^\bullet$ loss	X^- loss
F	125.3 (135)**	608.7	339.3	-176.1 (n.a.)	623.1	134.1
Cl	237.5 (245)	473.9	235.0**	-8.7 (-4.8)**	509.2	95.2
Br	257.9 (261)	421.0*	206.4**	33.1 (48)**	462.7	89.2*
I	214.9 (224)	356.7**	169.9*	76.2 (86)	409.3	82.8**

(c) PBE0-GD3BJ/def2-TZVPP

Substituent X	$[B_{12}X_{12}]^{2-}$			$[B_6X_6]^{2-}$		
	e^- loss	$X^\bullet$ loss	X^- loss	e^- loss	$X^\bullet$ loss	X^- loss
F	125.7 (135)**	593.6	352.4	-185.6 (n.a.)	613	155
Cl	223.8 (245)	479.4	251.7**	-29.0 (-4.8)**	515	110
Br	254.0 (261)	424.2*	224.5**	21.9 (48)**	467	105*
I	219.6 (224)	363.2**	188.4*	69.8 (86)	414	100**

(d) PBE0-GD3BJ/aug-cc-pVTZ

Substituent X	$[B_{12}X_{12}]^{2-}$			$[B_6X_6]^{2-}$		
	e^- loss	$X^\bullet$ loss	X^- loss	e^- loss	$X^\bullet$ loss	X^- loss
F	127.6 (135)**	594.2	351.6	-181.3 (n.a.)	611.9	154.4
Cl	237.6 (245)	476.8	253.7**	-10.6 (-4.8)**	514.6	115.2
Br	260.3 (261)	423.2*	223.4**	32.9 (48)**	467.3	107.6*
I	225.2 (224)	359.9**	184.4*	80.5 (86)	414.7	98.9**

Table S4. Calculated 0 K enthalpies for e^- and I^- loss from *closo*-$[B_6I_6]^{2-}$ on MP2, SCS-MP2, SOS-MP2/aug-cc-pVTZ (SDD for I for MP2) levels of theory. The reaction enthalpies were evaluated for geometries optimized on MP2 and PBE0 level. The results confirm that the conclusion drawn from thermochemistry calculations (I^- loss is not more favorable than e^- loss) are not an artifact of the employed DFT method but are also supported when post-HF methods such as MP2 are used. Enthalpies are given in kJ/mol.

(a) MP2 results (BSSE-corrected)

Energy//Geometry	e^- loss	I^- loss
MP2/aug-cc-pVTZ/SDD//MP2/aug-cc-pVTZ/SDD	69.6	76.2
MP2/aug-cc-pVTZ/SDD//PBE0/aug-cc-pVTZ/SDD	67.4	78.4

(b) SCS-MP2 and SOS-MP2 results (not BSSE-corrected)

Energy//Geometry	e^- loss	I^- loss
SCS-MP2/aug-cc-pVTZ// SCS-MP2/aug-cc-pVTZ	102.3	172.4
SOS-MP2/aug-cc-pVTZ// SOS-MP2/aug-cc-pVTZ	102.2	165.5

Table S5: Comparison of the experimental (PES) and theoretical (ESP based on PBE0-GD3BJ/aug-cc-pVTZ wave functions) results used to estimate the RCB height for *closo*-$[B_6X_6]^{2-}$. Results for $[B_{12}X_{12}]^{2-}$ ions were adopted from Ref. 26. Barrier heights are given in eV.

X	**PES (B_6)**	**PES (B_{12})**	**ESP(B_6)**	**ESP(B_{12})**
Cl	2.4-2.8	2.3-2.5	2.8	2.3
Br	2.0-2.3	2.1-2.3	2.4	2.1
I	1.9-2.3	1.8-2.3	2.1	1.9

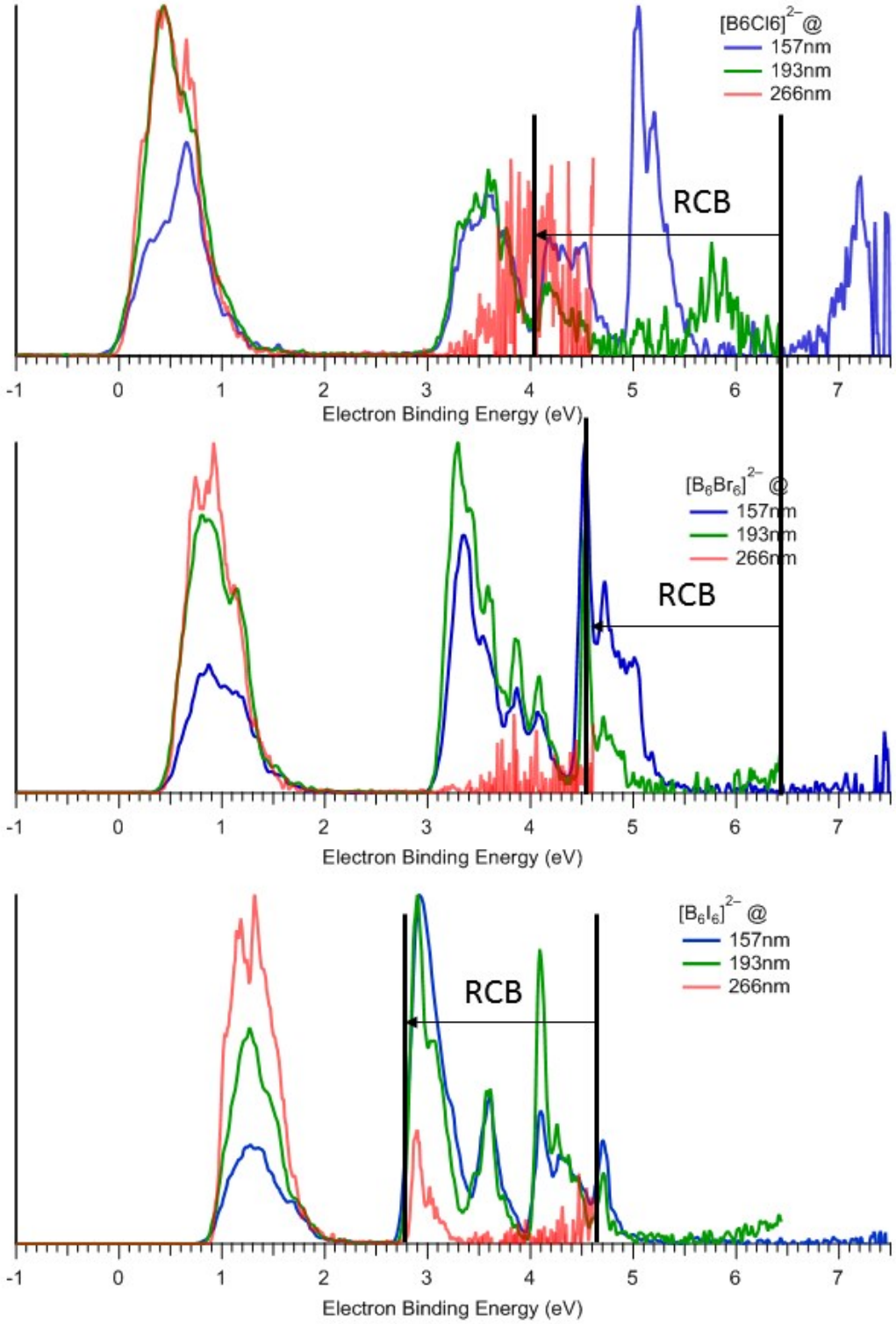

Figure S3. PES spectra for $[B_6Cl_6]^{2-}$, $[B_6Br_6]^{2-}$, and $[B_6I_6]^{2-}$ obtained with photons at three different wavelengths showing the influence of the RCB on the spectral feature intensity.

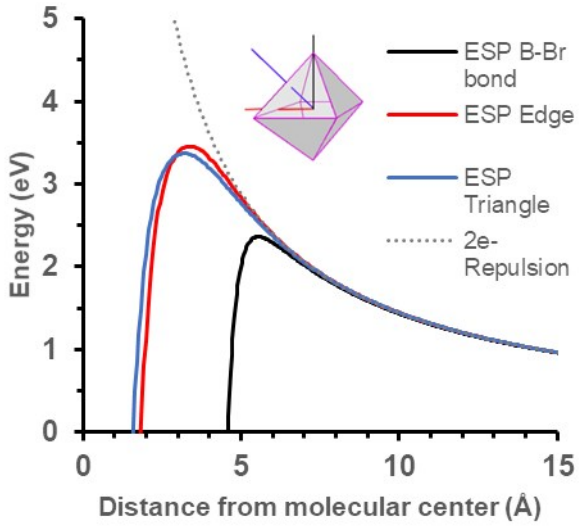

Figure S4. Results of computational investigations (PBE1PBE-GD3BJ/aug-cc-pVTZ) to determine the RCB for electron loss. The potential energy of a negative probing charge depending on the distance to the ion was calculated based on the ESP of $[B_6Br_6]^{\bullet-}$//$[B_6Br_6]^{2-}$. The geometry of the dianion was used in this calculation because electron loss is considered to be faster than geometry reoptimization. The potential energy was evaluated along three different electron detachment directions (1. B-Br, 2. B-B edge, 3. face of a boron triangle).

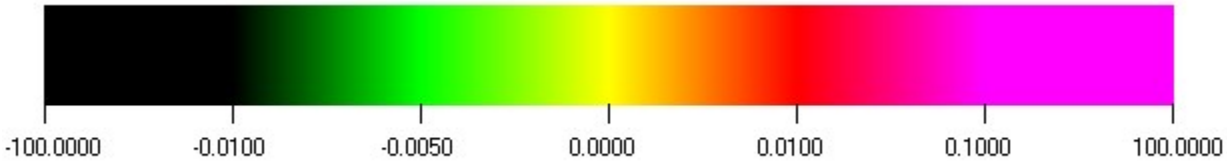

Figure S5. Color coding applied to Figure 6(b). Colors represent the magnitude of the electric field at a certain position with respect to the molecular center (see also Experimental and theoretical methodologies). The numbers below the color legend can be rationalized by considering that ESP cube files (unit: 1 a.u. = 1 Ha/e = 27.211 V) were numerically differentiated using difference quotient. The cube files employed here have a step size of 0.05 Å. Therefore, the unit of the electric field according to the color code is 1 = 27.211 V / $0.05*10^{-10}$ m = 5.4 TV/m = 5.4 TN/C (i.e., Tera Newton per Coulomb).

Table S6: Relaxation energies for various $[B_nX_{n-1}]^{-/2-\bullet}$ species after $X^{\bullet}/X^-$ loss, calculated on PBE1PBE-GD3BJ/aug-cc-pVTZ level. All energies are given in kJ/mol.

Substituent X	$[B_{12}X_{12}]^{2-}$		$[B_6X_6]^{2-}$	
	$X^{\bullet}$ loss	X^- loss	$X^{\bullet}$ loss	X^- loss
Cl	-5.4	-58.8	-0.7	-49.4
Br	-5.3	-57.4	-0.7	-48.4
I	-6.4	-55.5	-0.7	-47.6

Table S7. Properties of the B-X bond critical points (bcps) based on PBE1PBE-GD3BJ/aug-cc-pVTZ wave functions.

X =	F		Cl		Br		I	
Property	B6	B12	B6	B12	B6	B12	B6	B12
ρ_{bcp} / e Å^{-3}	1.038	1.163	0.820	0.913	0.755	0.833	0.679	0.720
$\nabla^2\rho_{bcp}$ / e Å^{-5}	22.880	24.773	2.654	0.875	-1.134	-3.343	-4.363	-3.860
H_{bcp}/ρ_{bcp} / Ha·e^{-1}	-0.618	-0.681	-0.863	-0.919	-0.876	-0.901	-0.714	-0.611

Table S8. Properties of the B-X bond critical points (bcps) based on B3LYP-GD3BJ/def2-TZVPP wave functions.

X =	F		Cl		Br		I	
Property	B6	B12	B6	B12	B6	B12	B6	B12
ρ_{bcp} / e Å^{-3}	1.015	1.143	0.812	0.913	0.744	0.830	0.680	0.722
$\nabla^2\rho_{bcp}$ / e Å^{-5}	20.789	22.919	-1.615	-0.358	-2.890	-5.123	-3.687	-3.635
H_{bcp}/ρ_{bcp} / Ha·e^{-1}	-0.640	-0.685	-0.902	-0.963	-0.910	-0.908	-0.634	-0.574

Table S9: B-X bond properties based on B3LYP-GD3BJ/def2-TZVPP wave functions. For RJI, the value stated corresponds to the percentage of electrons in the intersection region of atomic QTAIM basin and ELI-D bond basin assigned to the halogen atom.

X =	Cl		Br		I	
Property	B6	B12	B6	B12	B6	B12
d / Å	1.828	1.801	1.983	1.962	2.176	2.177
δ	0.66	0.66	0.72	0.76	0.88	0.91
Q_{AIM}(X) / e	-0.77	-0.71	-0.69	-0.58	-0.49	-0.33
Q_{NPA}(X)/ e	-0.24	-0.12	-0.18	-0.05	-0.11	+0.04
N (ELI) / e	1.55	1.58	1.53	1.58	1.55	1.62
RJI / %	87.25	85.09	82.01	76.47	69.61	60.71

Table S10. Cartesian coordinates (in Å) for $[B_6F_6]^{2-}$ optimized on PBE0-GD3BJ/aug-cc-pVTZ level of theory.

Atom	X	Y	Z
B	0.000000000	0.000000000	1.222995000
B	0.000000000	1.222995000	0.000000000
B	1.222995000	0.000000000	0.000000000
B	0.000000000	-1.222995000	0.000000000
B	-1.222995000	0.000000000	0.000000000
B	0.000000000	0.000000000	-1.222995000
F	0.000000000	0.000000000	2.636220000
F	0.000000000	2.636220000	0.000000000
F	2.636220000	0.000000000	0.000000000
F	0.000000000	-2.636220000	0.000000000
F	-2.636220000	0.000000000	0.000000000
F	0.000000000	0.000000000	-2.636220000

Table S11. Cartesian coordinates (in Å) for $[B_6F_6]^{\bullet-}$ optimized on PBE0-GD3BJ/aug-cc-pVTZ level of theory.

Atom	X	Y	Z
B	0.658246000	-0.972479000	0.410724000
B	-0.668351000	-0.841381000	-0.627134000
B	-0.652803000	-0.121691000	1.052127000
B	0.668254000	0.841461000	0.627119000
B	0.652753000	0.121743000	-1.052070000
B	-0.658371000	0.972498000	-0.410692000
F	1.528619000	-1.937088000	0.816126000
F	-1.549004000	-1.674269000	-1.246580000
F	-1.517425000	-0.241601000	2.095307000
F	1.548816000	1.674171000	1.246536000
F	1.517571000	0.241713000	-2.095401000
F	-1.528426000	1.936990000	-0.816028000

Table S12. Cartesian coordinates (in Å) for $[B_6F_5]^-$ optimized on PBE0-GD3BJ/aug-cc-pVTZ level of theory.

Atom	X	Y	Z
B	0.000000000	0.000000000	0.860484000
B	0.000000000	1.270499000	-0.307803000
B	1.270499000	0.000000000	-0.307803000
B	0.000000000	-1.270499000	-0.307803000
B	-1.270499000	0.000000000	-0.307803000
B	0.000000000	0.000000000	-1.383909000
F	0.000000000	0.000000000	2.243424000
F	0.000000000	2.639564000	-0.317156000
F	2.639564000	0.000000000	-0.317156000
F	0.000000000	-2.639564000	-0.317156000
F	-2.639564000	0.000000000	-0.317156000

Table S13. Cartesian coordinates (in Å) for $[B_6F_5]^{\bullet 2-}$ optimized on PBE0-GD3BJ/aug-cc-pVTZ level of theory.

Atom	X	Y	Z
B	0.000000000	0.000000000	0.905755000
B	0.000000000	1.225681000	-0.318019000
B	1.225681000	0.000000000	-0.318019000
B	0.000000000	-1.225681000	-0.318019000
B	-1.225681000	0.000000000	-0.318019000
B	0.000000000	0.000000000	-1.512307000
F	0.000000000	0.000000000	2.319030000
F	0.000000000	2.634985000	-0.318837000
F	2.634985000	0.000000000	-0.318837000
F	0.000000000	-2.634985000	-0.318837000
F	-2.634985000	0.000000000	-0.318837000

Table S14. Cartesian coordinates (in Å) for $[B_6Cl_6]^{2-}$ optimized on PBE0-GD3BJ/aug-cc-pVTZ level of theory.

Atom	X	Y	Z
B	0.000000000	0.000000000	1.209494000
B	0.000000000	1.209494000	0.000000000
B	1.209494000	0.000000000	0.000000000
B	0.000000000	-1.209494000	0.000000000
B	-1.209494000	0.000000000	0.000000000
B	0.000000000	0.000000000	-1.209494000
Cl	0.000000000	0.000000000	3.027328000
Cl	0.000000000	3.027328000	0.000000000
Cl	3.027328000	0.000000000	0.000000000
Cl	0.000000000	-3.027328000	0.000000000
Cl	-3.027328000	0.000000000	0.000000000
Cl	0.000000000	0.000000000	-3.027328000

Table S15. Cartesian coordinates (in Å) for $[B_6Cl_6]^{\bullet-}$ optimized on PBE0-GD3BJ/aug-cc-pVTZ level of theory.

Atom	X	Y	Z
B	0.652561000	1.040310000	0.040619000
B	-0.673959000	0.472774000	0.911975000
B	-0.671709000	0.541094000	-0.874998000
B	0.674175000	-0.472696000	-0.912146000
B	0.671802000	-0.541177000	0.875006000
B	-0.652183000	-1.040496000	-0.040755000
Cl	1.709381000	2.456764000	0.096151000
Cl	-1.761029000	1.113236000	2.150753000
Cl	-1.755520000	1.274753000	-2.063903000
Cl	1.761149000	-1.113627000	-2.150792000
Cl	1.755561000	-1.274676000	2.064078000
Cl	-1.709745000	-2.456393000	-0.096200000

Table S16. Cartesian coordinates (in Å) for $[B_6Cl_5]^-$ optimized on PBE0-GD3BJ/aug-cc-pVTZ level of theory.

Atom	X	Y	Z
B	0.000000000	0.000000000	0.696009000
B	0.000000000	1.263072000	-0.450975000
B	1.263072000	0.000000000	-0.450975000
B	0.000000000	-1.263072000	-0.450975000
B	-1.263072000	0.000000000	-0.450975000
B	0.000000000	0.000000000	-1.506992000
Cl	0.000000000	0.000000000	2.489777000
Cl	0.000000000	3.039945000	-0.430173000
Cl	3.039945000	0.000000000	-0.430173000
Cl	0.000000000	-3.039945000	-0.430173000
Cl	-3.039945000	0.000000000	-0.430173000

Table S17. Cartesian coordinates (in Å) for $[B_6Cl_5]^{\bullet 2-}$ optimized on PBE0-GD3BJ/aug-cc-pVTZ level of theory.

Atom	X	Y	Z
B	0.000000000	0.000000000	0.750159000
B	0.000000000	1.209667000	-0.461530000
B	1.209667000	0.000000000	-0.461530000
B	0.000000000	-1.209667000	-0.461530000
B	-1.209667000	0.000000000	-0.461530000
B	0.000000000	0.000000000	-1.662291000
Cl	0.000000000	0.000000000	2.581538000
Cl	0.000000000	3.036089000	-0.442572000
Cl	3.036089000	0.000000000	-0.442572000
Cl	0.000000000	-3.036089000	-0.442572000
Cl	-3.036089000	0.000000000	-0.442572000

Table S18. Cartesian coordinates (in Å) for $[B_6Br_6]^{2-}$ optimized on PBE0-GD3BJ/aug-cc-pVTZ level of theory.

Atom	X	Y	Z
B	0.000000000	0.000000000	1.206721000
B	0.000000000	1.206721000	0.000000000
B	1.206721000	0.000000000	0.000000000
B	0.000000000	-1.206721000	0.000000000
B	-1.206721000	0.000000000	0.000000000
B	0.000000000	0.000000000	-1.206721000
Br	0.000000000	0.000000000	3.173254000
Br	0.000000000	3.173254000	0.000000000
Br	3.173254000	0.000000000	0.000000000
Br	0.000000000	-3.173254000	0.000000000
Br	-3.173254000	0.000000000	0.000000000
Br	0.000000000	0.000000000	-3.173254000

Table S19. Cartesian coordinates (in Å) for $[B_6Br_6]^{\bullet-}$ optimized on PBE0-GD3BJ/aug-cc-pVTZ level of theory.

Atom	X	Y	Z
B	0.658526000	1.032840000	0.023151000
B	-0.671353000	0.487584000	0.900845000
B	-0.671543000	0.527661000	-0.878174000
B	0.671838000	-0.487487000	-0.901233000
B	0.671802000	-0.527796000	0.878107000
B	-0.657738000	-1.033118000	-0.023538000
Br	1.809866000	2.567450000	0.057726000
Br	-1.843799000	1.209708000	2.237285000
Br	-1.843959000	1.309815000	-2.180348000
Br	1.844109000	-1.210551000	-2.237367000
Br	1.843946000	-1.309620000	2.180760000
Br	-1.810381000	-2.566757000	-0.057936000

Table S20. Cartesian coordinates (in Å) for $[B_6Br_5]^-$ optimized on PBE0-GD3BJ/aug-cc-pVTZ level of theory.

Atom	X	Y	Z
B	0.000000000	0.000000000	0.594444000
B	0.000000000	1.261286000	-0.548181000
B	1.261286000	0.000000000	-0.548181000
B	0.000000000	-1.261286000	-0.548181000
B	-1.261286000	0.000000000	-0.548181000
B	0.000000000	0.000000000	-1.601308000
Br	0.000000000	0.000000000	2.538965000
Br	0.000000000	3.189077000	-0.520470000
Br	3.189077000	0.000000000	-0.520470000
Br	0.000000000	-3.189077000	-0.520470000
Br	-3.189077000	0.000000000	-0.520470000

Table S21. Cartesian coordinates (in Å) for $[B_6Br_5]^{\bullet 2-}$ optimized on PBE0-GD3BJ/aug-cc-pVTZ level of theory.

Atom	X	Y	Z
B	0.000000000	0.000000000	0.649966000
B	0.000000000	1.206455000	-0.560310000
B	1.206455000	0.000000000	-0.560310000
B	0.000000000	-1.206455000	-0.560310000
B	-1.206455000	0.000000000	-0.560310000
B	0.000000000	0.000000000	-1.762215000
Br	0.000000000	0.000000000	2.632913000
Br	0.000000000	3.183748000	-0.538461000
Br	3.183748000	0.000000000	-0.538461000
Br	0.000000000	-3.183748000	-0.538461000
Br	-3.183748000	0.000000000	-0.538461000

Table S22. Cartesian coordinates (in Å) for $[B_6I_6]^{2-}$ optimized on PBE0-GD3BJ/aug-cc-pVTZ/SDD level of theory.

Atom	X	Y	Z
B	0.000000000	0.000000000	1.204018000
B	0.000000000	1.204018000	0.000000000
B	1.204018000	0.000000000	0.000000000
B	0.000000000	-1.204018000	0.000000000
B	-1.204018000	0.000000000	0.000000000
B	0.000000000	0.000000000	-1.204018000
I	0.000000000	0.000000000	3.381751000
I	0.000000000	3.381751000	0.000000000
I	3.381751000	0.000000000	0.000000000
I	0.000000000	-3.381751000	0.000000000
I	-3.381751000	0.000000000	0.000000000
I	0.000000000	0.000000000	-3.381751000

Table S23. Cartesian coordinates (in Å) for $[B_6I_6]^{\bullet-}$ optimized on PBE0-GD3BJ/aug-cc-pVTZ/SDD level of theory.

Atom	X	Y	Z
B	0.666691000	1.022486000	-0.016697000
B	-0.671785000	0.522161000	0.875430000
B	-0.672036000	0.493456000	-0.891701000
B	0.671777000	-0.522183000	-0.875394000
B	0.672044000	-0.493464000	0.891712000
B	-0.666704000	-1.022502000	0.016734000
I	1.943014000	2.733537000	-0.044665000
I	-1.956929000	1.395185000	2.339576000
I	-1.957576000	1.318438000	-2.383119000
I	1.956920000	-1.395187000	-2.339558000
I	1.957660000	-1.318468000	2.383056000
I	-1.943089000	-2.733500000	0.044701000

Table S24. Cartesian coordinates (in Å) for $[B_6I_5]^-$ optimized on PBE0-GD3BJ/aug-cc-pVTZ/SDD level of theory.

Atom	X	Y	Z
B	0.000000000	0.000000000	0.518441000
B	0.000000000	1.259643000	-0.618558000
B	1.259643000	0.000000000	-0.618558000
B	0.000000000	-1.259643000	-0.618558000
B	-1.259643000	0.000000000	-0.618558000
B	0.000000000	0.000000000	-1.667204000
I	0.000000000	0.000000000	2.677070000
I	0.000000000	3.402076000	-0.583819000
I	3.402076000	0.000000000	-0.583819000
I	0.000000000	-3.402076000	-0.583819000
I	-3.402076000	0.000000000	-0.583819000

Table S25. Cartesian coordinates (in Å) for $[B_6I_5]^{\bullet 2-}$ optimized on PBE0-GD3BJ/aug-cc-pVTZ/SDD level of theory.

Atom	X	Y	Z
B	0.000000000	0.000000000	0.577191000
B	0.000000000	1.203151000	-0.631183000
B	1.203151000	0.000000000	-0.631183000
B	0.000000000	-1.203151000	-0.631183000
B	-1.203151000	0.000000000	-0.631183000
B	0.000000000	0.000000000	-1.834452000
I	0.000000000	0.000000000	2.774216000
I	0.000000000	3.393144000	-0.604356000
I	3.393144000	0.000000000	-0.604356000
I	0.000000000	-3.393144000	-0.604356000
I	-3.393144000	0.000000000	-0.604356000